Preprint typeset in JHEP style - PAPER VERSION FERMILAB-PUB-12-040-T

NLO Higgs boson production plus one and two jets using the POWHEG BOX, MadGraph4 and MCFM

John Campbell
Fermilab, Batavia, IL 60510, USA
E-mail: johnmc@fnal.gov

R. Keith Ellis
Fermilab, Batavia, IL 60510, USA
E-mail: ellis@fnal.gov

Rikkert Frederix
Institut für Theoretische Physik, Universität Zürich, Winterthurerstrasse 190, CH-8057 Zürich, Switzerland
E-mail: frederix@physik.uzh.ch

Paolo Nason
INFN, Sezione di Milano-Bicocca, Piazza della Scienza 3, 20126 Milan, Italy
E-mail: Paolo.Nason@mib.infn.it

Carlo Oleari
Università di Milano-Bicocca and INFN, Sezione di Milano-Bicocca
Piazza della Scienza 3, 20126 Milan, Italy
E-mail: Carlo.Oleari@mib.infn.it

Ciaran Williams
Fermilab, Batavia, IL 60510, USA
E-mail: ciaran@fnal.gov

Abstract: We present a next-to-leading order calculation of Higgs boson production plus one and two jets via gluon fusion interfaced to shower Monte Carlo programs, implemented according to the POWHEG method. For this implementation we have used a new interface of the POWHEG BOX with MadGraph4, that generates automatically the codes for the Born and real processes. The virtual corrections have been taken from the MCFM code. We carry out a simple phenomenological study of our generators, comparing them among each other and with fixed next-to-leading order results.

Keywords: QCD, Monte Carlo, NLO Computations, Resummation, Collider Physics

February 20, 2012 —9:04

.

Contents

1. Introduction

The search for the Standard Model Higgs boson is entering the endgame phase. Since the start of the LHC running, the allowed mass range for the standard model Higgs boson has been greatly curtailed. Furthermore there are tantalizing, but inconclusive, hints in the remaining low mass region [1, 2]. Should these hints be confirmed by further data, it will be a matter of some urgency to examine the properties of the new state (or states). In the low mass region, the Standard Model Higgs boson is predicted to have about ten branching ratios with branching fractions greater than one per mille, so there will a number of channels to be studied.

In order to extract the Higgs couplings from these different channels, detailed information about the production rates will be required [3, 4, 5]. In this context the Higgs + 2 jet process enters principally as an irreducible background for the Vector Boson fusion process. In fact applying cuts appropriate for the search for the vector boson fusion process, it is

found that the Higgs + 2 jet process from gluon fusion contributes more than 25% of the signal [6]. It is therefore of importance to provide NLO predictions for the gluon-fusion initiated Higgs + 2 jet process in a form that the experimenters can easily use.

The Higgs boson search channels are often subdivided in this manner, according to the number of associated yets, for a number of reasons. First, a differing number of associated jets can imply a different source of background. For example, in the search for a Higgs boson decaying to W^+W^- the backgrounds have different origins in the differing jet bins, so it proves advantageous to analyze the different jet multiplicities separately. Second, in the two jet bin, a new production channel, vector boson fusion will come into play. For these reasons it is pressing to provide predictions for these processes in the POWHEG formalism in such a way that the experimenters can incorporate the best theoretical information into their analyses.

Phenomenological studies for the production of a Higgs boson in association with two jets, at the parton level and without a hadron shower, have been presented for the LHC operating at $\sqrt{s} = 10$ TeV [6] and $\sqrt{s} = 14$ TeV [7].

In this work we have implemented Higgs boson plus one and two jet production in gluon fusion using the POWHEG method. While for the first process a matched NLO+shower calculation has already appeared in a publication [8], the second one has never been performed before. We have built our generators using the POWHEG BOX framework [9], with the virtual corrections taken from the MCFM program [10], and the Born , colour-correlated Born, spin-correlated Born and real contributions computed using a new POWHEG BOX interface to the MadGraph4 [11, 12] program, which is fully generic and can be applied to any process. Thus, the aim of this paper is twofold:

- To present a new generic interface of MadGraph4 to the POWHEG BOX that allows for the automatic generation of code for the Born, Born colour- and spin-correlated squared amplitudes, for the real-radiation amplitude and for the Born-colour flow at leading colour approximation. These ingredients are all needed in the implementation of a new process in the POWHEG BOX. This interface can be used for any process that can be generated with MadGraph4. Thanks to this interface, in order to construct a POWHEG BOX generator, one needs only to provide the Born phase space, and the virtual corrections.

- To illustrate the Higgs plus one and two jets generators, by comparing their output to the corresponding NLO results and amongst themselves.

2. The interface to MadGraph4

We have built a generic interface of the POWHEG BOX to the MadGraph4 package, for the construction of all the ingredients listed in the introduction of ref. [9], with the exception of the Born phase space and of the virtual matrix elements.

The MadGraph4 package [11, 12] generates squared tree-level matrix elements in an automatic way. It is based on Feynman diagrams which are constructed HELAS subroutines [13] using as building blocks and that are combined into colour-ordered amplitudes

which are written in a FORTRAN code. Furthermore, the MadDipole [14, 15, 16] extension of MadGraph4 and the MadFKS tool [17] can generate the Born spin- and color-correlated squared amplitudes, which makes the MadGraph4 framework an ideal environment to complement the POWHEG BOX in the creation of all tree-level squared matrix elements. In this section we describe a newly developed interface between these two codes.

For a given process, the routines and parameters that are generated by MadGraph4 for the POWHEG BOX are (see ref. [9] for more details on the notation and conventions used)

- the multiplicity of the Born and real emission processes, `nlegborn` and `nlegreal`, respectively, defined in the `nlegborn.h` include file;

- the list of Born and real-emission flavour structures
  `flst_born(k=1,nlegborn,j=1:flst_nborn)`,
  `flst_real(k=1,nlegreal,j=1:flst_nreal)`,
  respectively, to be initialised by a call to the `init_processes` routine;

- the routine
  ```
  setborn(p(0:3,1:nlegborn),bflav(1:nlegborn),born,
          bornjk(1:nlegborn,1:nlegborn),bmunu(0:3,0:3,1:nlegborn))
  ```
  which computes, for a given set of four-momenta `p` and flavour structure `bflav`, the Born squared matrix element `born`, the colour-correlated, `bornjk`, and the spin-correlated one, `bmunu`;

- the routine that computes the real emission squared matrix elements `amp2`, (stripped of a factor $\alpha_{\rm S}/(2\pi)$), for a given momentum configuration `p` and flavour structure `rflav`
  `setreal(p(0:3,nlegreal),rflav(1:nlegreal),amp2)`;

- a colour flow assignment to the Born squared matrix elements, in the leading colour approximation, needed by the showering programs. The colour assignment is done on statistical grounds, based on information that is cached during the call to the squared matrix elements, by the routine `borncolour_lh`. In addition to the this routine, the interface provides also a similar one for the real squared matrix elements, `realcolour_lh`, not used by the present version of the POWHEG BOX, that uses its own method to assign the colour to the real-radiation matrix elements, as discussed in section 8 of ref. [9].

- an interface to the Les Houches parameter input card to specify the physics model parameters through a routine `init_couplings`.

In distinction to the default way of generating amplitudes with MadGraph4, all the squared matrix elements for the various flavour structures are written in the same directory, making sure that the files and routines have different names. This allows one to compile the code into a single library that contains all the matrix elements for all the flavour structures. An interface is provided that concatenates the flavour vectors `bflav` and `rflav` into strings, which are used as unique identifiers of each of the squared matrix elements.

More technical details on the use of the MadGraph4 interface to the POWHEG BOX can be found in Appendix A.

3. Higgs boson production in gluon fusion

In this paper we present results for the production of a Higgs boson in association with one and two jets, at NLO, interfaced with a parton shower using the POWHEG method. The basic hard cross sections for a Higgs boson in association with three, four or five partons, needed for the Higgs boson plus one and two jet cross sections at NLO are calculated using an effective Lagrangian to express the coupling of the gluons to the Higgs field [18]

$$\mathcal{L}_H = \frac{C}{2} H \ \mathrm{tr}\, G_{\mu\nu} G^{\mu\nu} \,, \tag{3.1}$$

where the trace is over the color degrees of freedom. At the order required in this paper, the coefficient C is given in the $\overline{\mathrm{MS}}$ scheme by [19, 20]

$$C = \frac{\alpha_{\mathrm{S}}}{6\pi v} \left(1 + \frac{11}{4\pi}\alpha_{\mathrm{S}}\right) + \mathcal{O}(\alpha_{\mathrm{S}}^3) \,, \tag{3.2}$$

where v is the vacuum expectation value of the Higgs field, $v = 246$ GeV.

We have used the automatic interface described in sec. 2 to generate the code for the Born, Born colour- and spin-correlated amplitudes and for the real cross section. In appendix A we give some more detailes on the adopted procedure. The one-loop amplitudes for the Higgs boson plus three and four parton processes are extracted from MCFM as described below.

3.1 Virtual cross section

The complete set of one-loop amplitudes for all Higgs + 4 parton processes are now available [21, 22, 23, 24, 25, 26, 27]. These formulae have been implemented into MCFM [6].

The interface between MCFM and the POWHEG BOX is fairly straightforward. The virtual pieces share the same phase space as the Born contributions. Since in the POWHEG implementation the Born, real and subtraction terms are provided elsewhere, MCFM needs only to return the pure virtual contributions. The interface to MCFM transfers the electroweak parameters, scale and scheme choices. Once these are established, calls to the virtual routines of MCFM can be made on an event-by-event basis.

Since the routines that fill the values of the electroweak parameters etc. are generic, this interface could be fairly easily extended to include other processes currently implemented in MCFM. However the normal MCFM routines are designed to return matrix elements that are summed over the flavour of the final state partons. Therefore in order to correctly interface to the POWHEG BOX one must make small modifications to the MCFM code such that it returns the matrix elements for individual final state flavour combinations.

4. Implementation of the Hj and Hjj generators

Using the automated MadGraph4interface described in the previous section, we have built the routines for the Born, color- and spin-correlated Born, and the real squared amplitudes, directly in the format required by the POWHEG BOX. The generation of the amplitudes is fast, taking only a few minutes for the Hjj process. The virtual corrections were extracted from the MCFM code. At this point, the only missing ingredient for completing our generators is the Born phase space.

4.1 Phase space for the Hj generator

The phase space routine for the Hj Born process is trivial, since it is just a two-body phase space. It has been implemented with the possibility to activate an optional cut on the transverse momentum of the Higgs, and with an effective importance sampling of the small transverse momentum region. The cut is necessary if one wants to generated unweighted events. Alternatively the cut can be set to zero, and the cross section is weighted with a suppression factor, that is a function of the underlying Born kinematics. This factor is equal to

$$F = \frac{p_T^2}{p_0^2 + p_T^2}\,, \tag{4.1}$$

where p_T is the Higgs transverse momentum in the underlying Born configuration and p_0 is set by the user [1]. Events are then generated uniformly in the cross section times F, and with a weight proportional to $1/F$. The normalization of the weight is such that the cross section for events passing a set of cuts is given by the sum of all weights for the events passing the cut divided by the total number of generated events.

4.2 Phase space for the Hjj generator

The phase space for the Hjj generator was built using the same factorized phase space that POWHEG uses for the real kinematics. In other words, we treat the Hjj Born phase space as the real phase space for the Hj process with one extra emission. Furthermore, we have allowed for the possibility to perform importance sampling in the region where the Born cross section becomes singular. More in detail, labeling with 1 and 2 the two final state light partons in the Hjj process, we write the Hjj phase space using the following identity

$$d\Phi_{H12} = d\Phi_{H12}\,\frac{N}{d_{12}}\,\frac{E_1}{E_1+E_2} + d\Phi_{H12}\,\frac{N}{d_{12}}\,\frac{E_2}{E_1+E_2} + d\Phi_{H12}\,\frac{N}{d_1} + d\Phi_{H12}\,\frac{N}{d_2}\,, \tag{4.2}$$

where E_i is the energy of the i-th parton in the center-of-mass frame, and

$$N = \left(\frac{1}{d_{12}} + \frac{1}{d_1} + \frac{1}{d_2}\right)^{-1} \tag{4.3}$$

[1] The value of p_0, set to 20 GeV for the simulation done in this paper, or the form of the suppression factor F in eq. (4.1), can be changed by the user by modifying the born_suppression routine in the Born_phsp.f file.

where d_1, d_2 and d_{12} are phase-space functions that vanish respectively when parton 1 is collinear to the initial state, parton 2 is collinear to the initial state, and parton 1-2 are collinear to each other. Their precise form is given in eqs. (4.23)-(4.26) of ref. [9]. We then factorize each phase space factor in (4.2) according to the formula

$$\begin{aligned} d\Phi_{H12} = {} & d\Phi_{H2}\, d\Phi_{\rm rad}^{(21)}\, \frac{N}{d_{12}}\, \frac{E_1}{E_1+E_2} + d\Phi_{H1}\, d\Phi_{\rm rad}^{(12)}\, \frac{N}{d_{12}}\, \frac{E_2}{E_1+E_2} \\ & + d\Phi_{H2}\, d\Phi_{\rm rad}^{(01)}\, \frac{N}{d_1} + d\Phi_{H1}\, d\Phi_{\rm rad}^{(02)}\, \frac{N}{d_2}\,. \end{aligned} \tag{4.4}$$

The subscripts $H1$ or $H2$ characterize the underlying Born, while the superscript in $\Phi_{\rm rad}$ specifies the radiation process. Thus, for example, $d\Phi_{H2}$ is the underlying Born phase space of the Higgs together with parton 2, and $d\Phi_{\rm rad}^{(21)}$ is the radiation phase space corresponding to parton 2 emitting parton 1. The notation $d\Phi_{\rm rad}^{(01)}$ or $d\Phi_{\rm rad}^{(02)}$ means that partons 1 or 2 are emitted by the initial state partons. The factorization of the phase space into underlying Born and radiation phase space for both initial and final state radiation is the default one used in `POWHEG`, and is described in detail in section 5.1 and 5.2 of ref. [28]. The decomposition in eq. (4.4) is such that appropriate importance sampling is performed in all singular regions. In fact, the factors in each term damp all but one singular region, and the corresponding factorized phase space performs importance sampling precisely in that region. Ideally, the phase space integration should be performed with an integrator that can sum over a discrete variable. The `POWHEG BOX` integrator [29] does not have this feature at the moment. Thus, we divided the range of one extra integration variable into four segments, mapping each segment to one of the phase space components.

The phase space of eq. (4.4) is not the default one used in the Hjj generator. It is activated by setting the variable `fullphsp` in the `powheg_input` file. The default phase space is simply

$$d\Phi_{H12} = d\Phi_{H1}\, d\Phi_{\rm rad}^{(02)}\,, \tag{4.5}$$

with no importance sampling at all. We have in fact observed that the loss of efficiency due to the increased number of calls to the matrix element routines overwhelms any benefit arising from the improved importance sampling.

As for the case of the Hj generator, the Hjj generator also includes the implementation of a Born suppression factor for the suppression of the singularities of the underlying Born in the `born_suppression` routine. It has the form

$$F = \left(\frac{1/p_0^2}{1/p_{T1}^2 + 1/p_{T2}^2 + 1/p_{T12}^2 + 1/p_0^2} \right)^2, \tag{4.6}$$

where p_0 is a parameter that characterizes the minimum jet energy where some accuracy is required, p_{T1} and p_{T2} are the transverse momenta (with respect to the beam axis) of the two final state partons, and

$$p_{T12}^2 = 2(1-\cos\theta_{12})\, \frac{E_1^2\, E_2^2}{E_1^2+E_2^2}\,, \tag{4.7}$$

that can be interpreted as the transverse momentum of parton 1 with respect to parton 2 or vice-versa, depending upon which is the softest. This suppression factor can also play the role of a generation cut, if p_0 is chosen small enough.

4.3 The POWHEG BOX parameter setting

We have turned on the `bornzerodamp` flag by default in both the Hj and the Hjj generators. The purpose of this flag is explained in ref. [9]. This results in a considerable speedup of the Hjj code. However, no appreciable differences were observed in the distribution obtained without the `bornzerodamp` option.

The separation of the singular regions is controlled in the POWHEG BOX by the parameters `par_diexp` and `par_dijexp` that are set to 1 by default (see ref. [9], section 4.7). In the generators at hand we have preferred to set them to 2, which leads to slightly better stability for the set of distributions that we have considered. We notice that also in the POWHEG BOX dijet generator [30] these parameters were set to 2. Higher values of these parameters correspond to sharper separation of singular regions.

5. Phenomenology

In this section, we present a phenomenological study of our generators. This study does not aim to produce results with realistic experimental cuts, but rather to compare the output of the generators in the description of some key observables. In particular, we compare the generator results to the fixed NLO result and with the POWHEG output at the level of the generation of the hardest radiation (i.e. before interfacing the result to a parton shower program), after the shower with no hadronization effects, and after hadronization. In the following, we use the notation H, Hj and Hjj to refer to Higgs boson generators that, at the Born level, describe the production of a Higgs boson plus zero, one and two partons.

We present results for the LHC running at 7 TeV, computed using the CTE6M parton distribution function (pdf) set [31]. The same calculations can easily be performed with any other available set [32, 33], but a study of pdf effects is beyond the scope of the present paper. Jets are reconstructed using the anti-$k_{\rm T}$ jet algorithm [34], with $R = 0.5$ and default recombination scheme. Cuts of 20, 50 and 100 GeV on the final-state jets are considered.

The factorization- and renormalization-scale choice deserves some more detailed discussion. In view of the large NLO corrections for the processes at hand, the scale dependence is quite large. This is also a consequence of the fact that Higgs boson production in gluon fusion starts at order $\alpha_{\rm S}^2$, so that the Hj and the Hjj processes are of order $\alpha_{\rm S}^3$ and $\alpha_{\rm S}^4$, respectively. While for H production the natural scale choice is of the order of the Higgs boson mass, in the case of Hj production one may have a two-scale problem if the transverse momentum of the jet is much smaller or much larger than the Higgs boson mass. In addition, besides the Higgs boson mass, one may also consider the Higgs boson transverse momentum, which may be more appropriate for very small or very large Higgs boson transverse momentum p_T^H, or the Higgs boson transverse mass $m_T^H = \sqrt{m_H^2 + p_T^2}$, which may be more appropriate for large Higgs boson transverse momentum. For the Hjj case, there are even more possibilities. Although a full study of scale dependence would be very valuable, we will not perform it in the present work. In the H case we will limit ourselves to the fixed Higgs boson mass scale choice, and p_T^H choice at the underlying-Born level. In the Hjj case we will consider the fixed Higgs boson mass scale choice, and the $\hat{H}_T$ scale

choice at the underlying Born level, where

$$\hat{H}_T = m_T^H + \sum_i p_{Ti} \tag{5.1}$$

and p_{Ti} are the final-state parton transverse momenta. All results shown in the following have been computed with $m_H = 120$ GeV.

In the following, we will label "LHE" the results obtained at the level of the POWHEG first emission, "PY" the results obtained with the POWHEG+PYTHIA combination with the hadronization and underlying event switched off, and with "NLO" the pure NLO results.

For some observables, there is overlap among the various generators. For example, the Higgs boson transverse momentum, as well as the one-jet multiplicity and the transverse momentum of the leading jet, are described by both the H and the Hj generators. The H generator gives a plausible description for these quantities also at small transverse momenta, since it provides a resummation of transverse momentum logarithms that the Hj program does not provide. On the other hand, at large transverse momenta, the Hj generator has NLO accuracy, something that the H generator does not have. For the same quantities, the Hjj generator cannot be used, since it requires the presence of a second jet. The two-jet multiplicity, as well as the second hardest jet transverse-momentum distribution, are provided by both the Hj and the Hjj programs, again with a different level of accuracy. A comparison of the generators in the regions where they overlap will also be carried out.

5.1 Results for Hj production

We have simulated Hj production with two scale choices: $\mu_{\rm F} = \mu_{\rm R} = m_H$ and the p_T of the underlying Born parton $\mu_{\rm F} = \mu_{\rm R} = p_T^{\rm UB}$. All the following plots will come in pairs, with the left plot referring to $\mu_{\rm F} = \mu_{\rm R} = m_H$, and the right one to $\mu_{\rm F} = \mu_{\rm R} = p_T^{\rm UB}$. We compare the fixed NLO results, the POWHEG hardest-emission results (LHE) and POWHEG+PYTHIA (PY) ones, where hadronization and underlying event in PYTHIA have been turned off (see Appendix B). For a few physical observables, we show results for three different cuts applied to the final-state jets: p_T cuts of 20, 50 and 100 GeV.

In fig. 1 we compare the jet multiplicity for one and two jets, at NLO, LHE and PY level, for jet cuts of 20, 50 and 100 GeV. We notice that the one-jet multiplicity is similar in the three results. Understandably the PYTHIA multiplicity is smaller than the LHE, due to showering off the first jet. More marked differences can be seen in the cross section of the second jet: here the LHE result is definitely larger than the NLO one, showing however a very different pattern as a function of the jet cut, depending upon the scale choice. We will clarify the origin of these patterns later, when we discuss the transverse-momentum spectrum of the jets. We point out, however, that the NLO result for the two-jet multiplicity is of order $\alpha_{\rm S}^4$, and has thus a marked scale dependence. For $p_T^j > 20$ GeV, the factorization scale is of the order of 20 GeV in the right plot, while it is the Higgs boson mass in the left plot, which justifies the large difference in the corresponding NLO results.

In fig. 2 we show the transverse momentum of the Higgs boson. The LHE, the PY and the NLO results are in remarkable agreement for this quantity, which is expected,

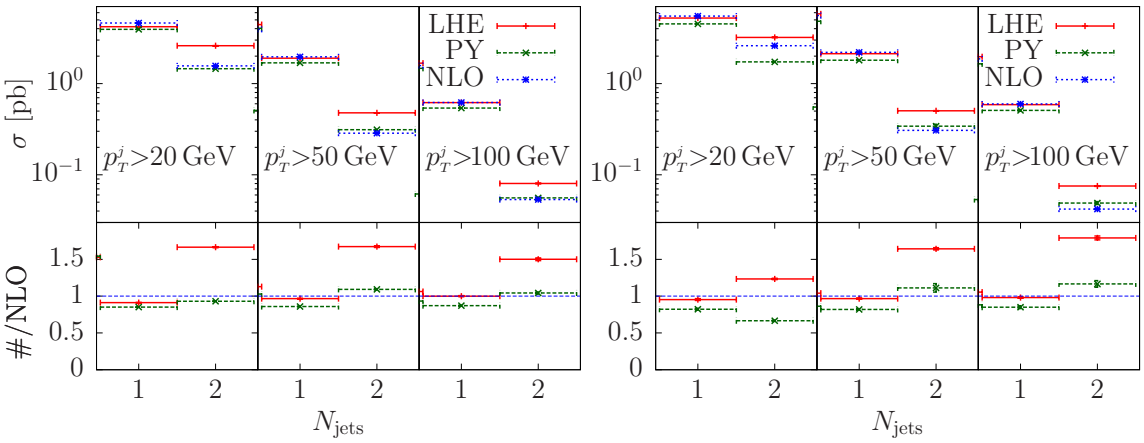

Figure 1: One- and two-jet multiplicities for the POWHEG hardest-emission (LHE) results, the POWHEG events showered with PYTHIA (PY) and the fixed NLO result (NLO). The left plot is computed using $\mu_{\rm F} = \mu_{\rm R} = m_H$, while in the right plot $\mu_{\rm F} = \mu_{\rm R} = p_T^{\rm UB}$.

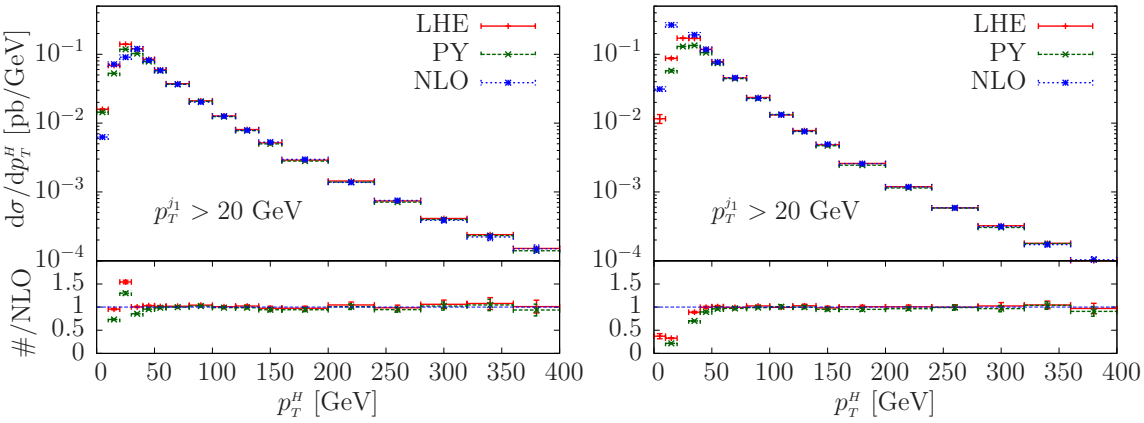

Figure 2: Transverse momentum of the Higgs boson. The notation is as in fig. 1.

due its inclusiveness. The Higgs boson rapidity distribution is plotted in fig. 3 while the hardest jet p_T in fig. 4. Both these quantities display a behaviour similar to the Higgs boson transverse momentum, again expected due to their inclusiveness.

We now turn to more exclusive quantities, beginning with the transverse momentum of the second jet, shown in fig. 5. The characteristic NLO behaviour, diverging at small transverse momenta, is clearly visible in the insert. The LHE result displays, instead, the typical Sudakov damping at small p_T, compensated by an increase at larger p_T. The fully showered result is smaller, since further showering degrades the second jet transverse momentum. The two-jet multiplicity displayed in fig. 1 is consistent with the value of the cross section around $p_T = 20$ GeV in fig. 2. From the upper insert in the figure, we see that, at this value of transverse momentum, the LHE cross section is above the NLO one for the fixed-scale choice (left plot), while it is near to it for the running-scale choice (right

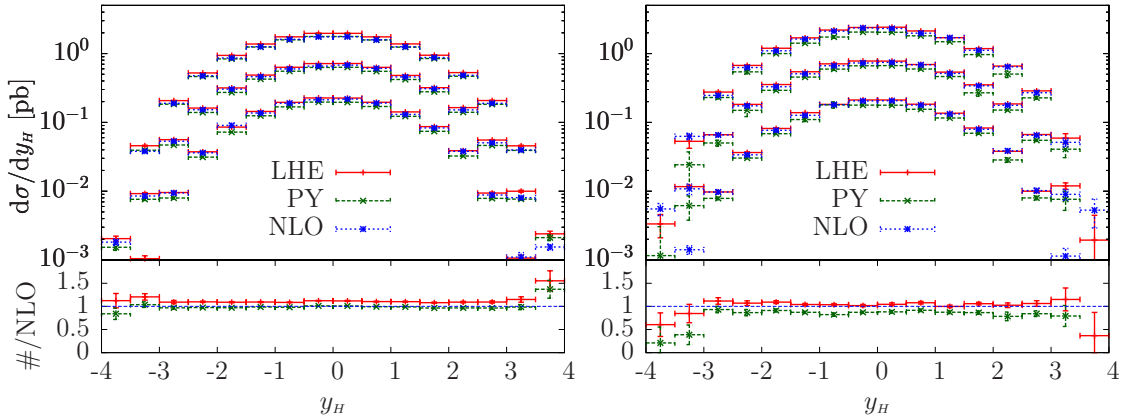

Figure 3: Rapidity distribution of the Higgs boson in the Hj process. The three sets of curves refer to the three cuts on the hardest jet, i.e. $p_T^{j_1} > 20$, 50 and 100 GeV, from top to bottom respectively.

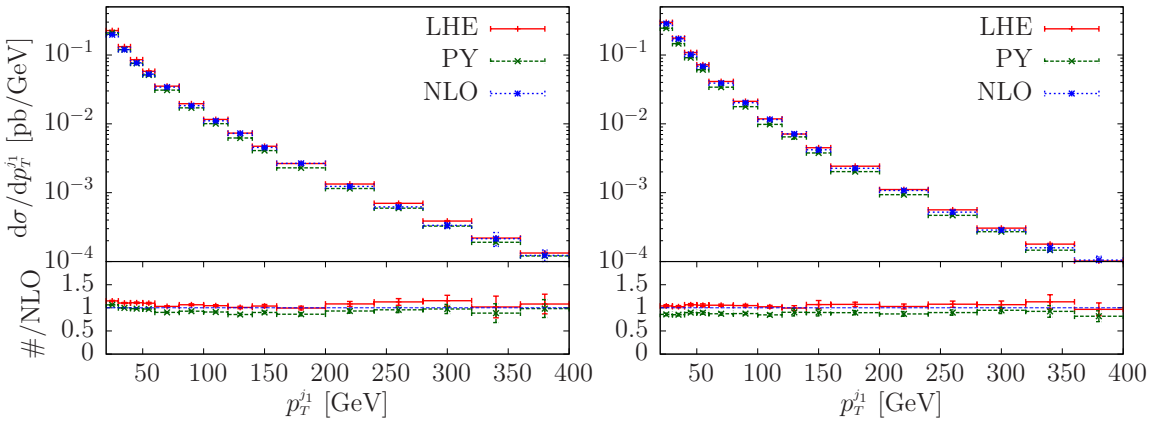

Figure 4: The hardest jet distribution in the Hj process.

plot). For larger p_T cuts, the LHE cross section remains above the NLO one in both cases, with a growing trend in the running scale case. The comparison of the fixed-scale and running-scale choice in the figure also has some subtle features that should be remarked upon. The running scale choice yields smaller/larger scales for small/large second jet p_T. The LO cross section is larger for smaller scale choices, so that the NLO corrections are smaller, and vice-versa for larger scale choices. Thus, for small p_T, the NLO corrections are smaller than for large p_T. In `POWHEG`, one first generates the underlying Born configuration, according to the cross section $\bar{B}$, which is the total inclusive cross section at fixed underlying Born configuration. The radiation kinematics is then generated using a shower technique. It thus turns out that the whole distribution for the radiation is amplified by a $\bar{B}/B$ K-factor [35, 36, 37]. In this case, due to the growth of the NLO corrections as a function of p_T, the amplification of the radiated jet distribution due to the $\bar{B}/B$ K-factor increases as a function of the transverse momentum, a trend that is visible in the right figure. Conversely, no such effect is present for fixed scales. However, in this last case, one should recall that,

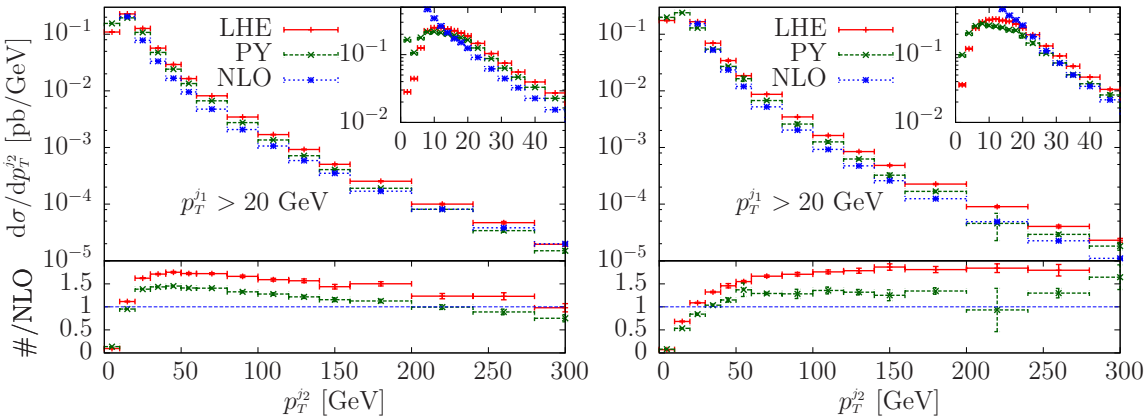

Figure 5: Transverse-momentum distribution of the second hardest jet in the Hj process, with a 20 GeV cut on the transverse momentum of the first jet.

in the LHE events, one power of α_S is effectively evaluated at the transverse momentum of the jet rather than at the fixed scale, thus yielding a decrease in the cross section which is also visible in the left plot. The larger value of the LHE cross section with respect to the NLO one is related to the large K-factor, i.e. is due to the fact that the hardest radiation is amplified by a factor $\bar{B}/B$.

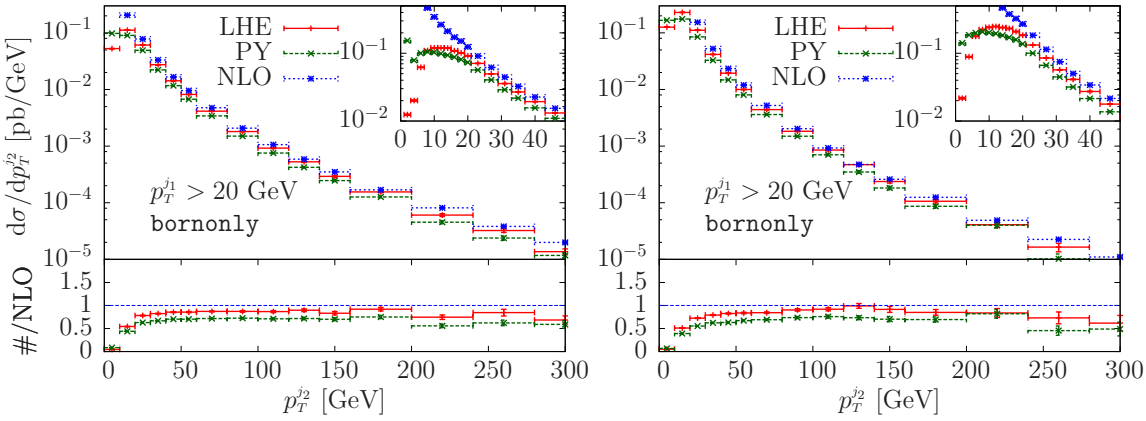

Figure 6: Transverse momentum distribution of the second hardest jet using the $\bar{B} \to B$ option.

Figure 6 is similar to fig. 5 except that the LHE result is obtained setting the `bornonly` flag to true in the `POWHEG BOX` input file. When this flag is true, the `POWHEG BOX` generator uses the Born cross section, rather than the NLO $\bar{B}$ function, to generate the underlying Born configuration. We can see that, in this case, the LHE result is much closer to the NLO result, except for small transverse momenta, where Sudakov damping becomes manifest. This results confirms that the enhancement of the transverse-momentum distribution of the second hardest jet is indeed due to the $\bar{B}/B$ K-factor.

In fig. 7 we show the second hardest jet transverse momentum for different cuts on

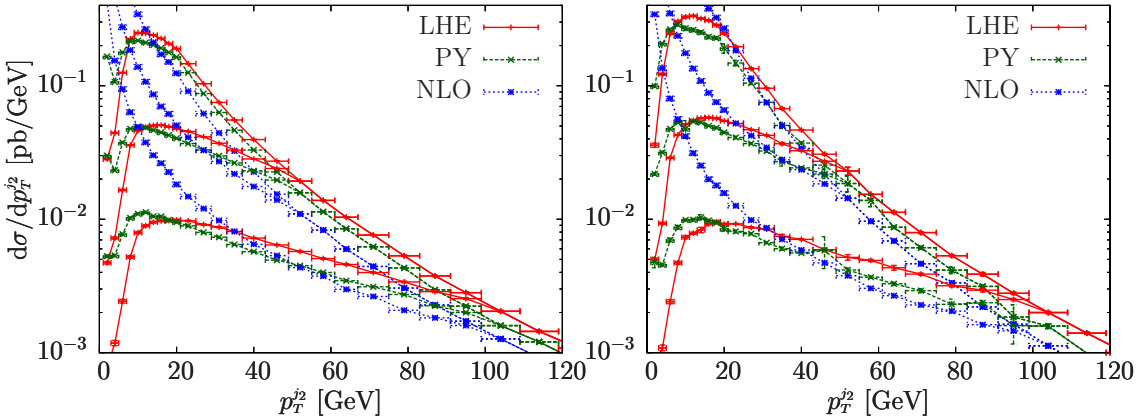

Figure 7: Transverse momentum distribution of the second hardest jet for different cuts on the first jet transverse momentum.

the first jet p_T. From the figure it is clear that, as long as the second jet p_T is below the first jet p_T cut, the behaviour of the cross section is roughly as an inverse power of the second jet transverse momentum. By raising the transverse momentum above the first jet p_T cut, also the first jet is forced to have larger transverse momentum, and the cross section falls much more rapidly. The comparison among the LHE, PY and NLO curves shows the typical pattern, with the NLO diverging at small transverse momenta, the LHE being instead suppressed in that region, but raising above the NLO result because of the $\bar{B}/B$ K-factor.

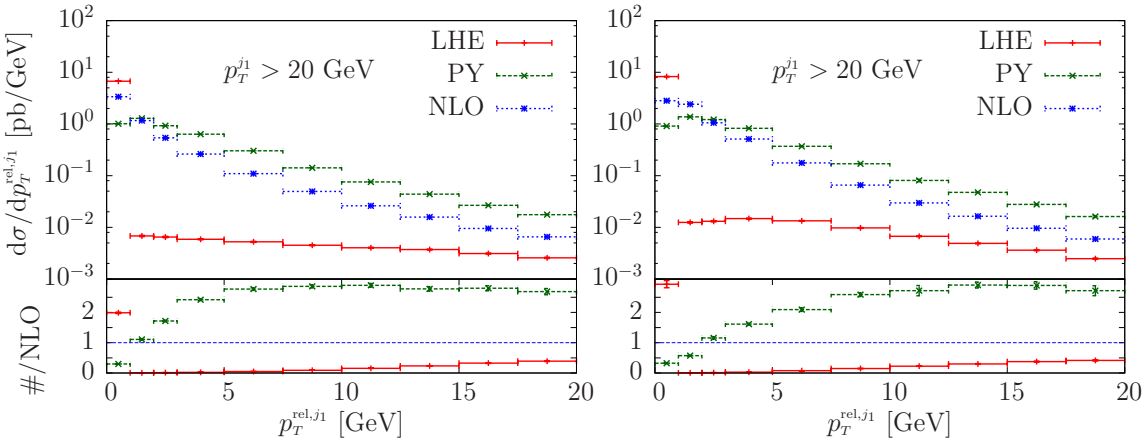

Figure 8: The relative transverse momenta of the partons within the hardest jet p_T^{rel,j_1} as defined in eq. (5.2).

In fig. 8 we plot the relative transverse momenta of the partons within the hardest jet p_T^{rel,j_1}. This quantity is defined as follows: we perform a longitudinal boost to a frame

where the rapidity of the first jet j_1 is zero. In this frame we compute

$$p_T^{\mathrm{rel},j_1} = \sum_{i \in j_1} \frac{|\vec{p}_i \times \vec{k}_j|}{|\vec{k}_j|}\,, \tag{5.2}$$

where k_j is the momentum of the first jet in this frame, and p_i the momenta of the partons clustered within the first jet. This quantity, when computed at the LHE level, displays a marked difference from the corresponding NLO result. As discussed in ref. [30], this can be easily understood if we remember that the LHE result is suppressed by a Sudakov form factor that requires that no hardest radiation has been emitted from either the initial- or the final-state partons. The large bin at $p_T^{\mathrm{rel},j_1} = 0$ in the LHE result is due to events where there is only one parton in the jet, that are most likely ISR events. On the other hand, the hardest radiation provided by `PYTHIA` should restore a shape closer to the NLO result, although amplified by the $\bar{B}/B$ factor. Further amplification of the showered result is due to the fact that the shower uses a running coupling evaluated at the scale of the radiation, while the NLO result uses higher scales, and to the presence of multiple emissions in the shower. It is clear that this distribution, being determined mostly by the shower program, is quite sensitive to the shower model and tuning, and to the interface between the shower and `POWHEG BOX`.

5.2 Results for Hjj production

We have run the Hjj program for two scale choices, $\mu_{\rm F} = \mu_{\rm R} = m_H$ and $\mu_{\rm F} = \mu_{\rm R} = \hat{H}_T$. All the following plots will come in pairs, the left one referring to the first scale choice, and the right one referring to the second scale choice.

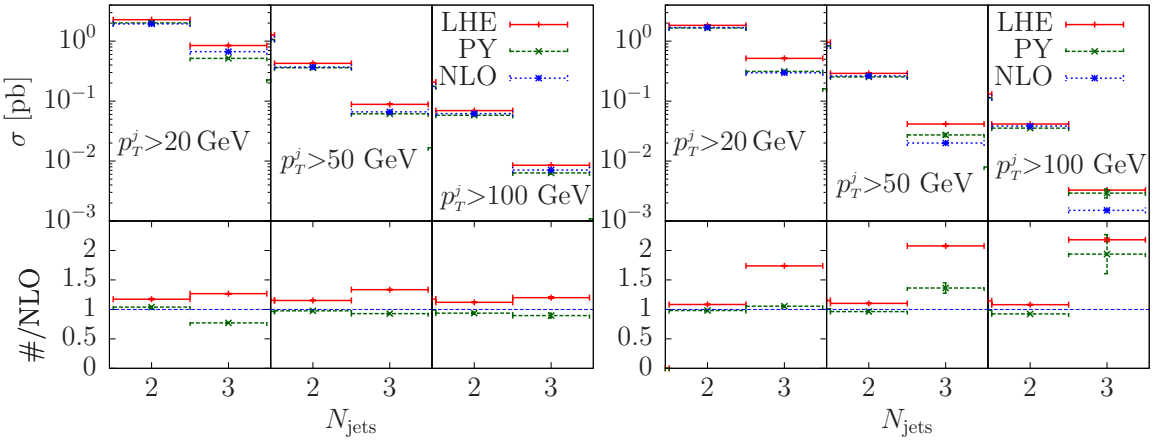

Figure 9: Two and three jet multiplicities in Hjj production. In the left plot the scale is chosen equal to the mass of the Higgs. In the right plot the scale is taken equal to $\hat{H}_T$.

We begin by showing in fig. 9 the two and three jet multiplicities in the Hjj process. We find considerable agreement of the LHE, PY and NLO output for both the two and three jet multiplicities for the left plot, which corresponds to the choice of scale $\mu_{\rm F} = \mu_{\rm R} = m_H$. The right plot corresponds to the $\hat{H}_T$ choice of scale. In this plot the two jet multiplicity agrees for all cuts, while the three-jet multiplicity displays marked differences between the LHE result and the NLO, and for the 100 GeV transverse momentum cut, also between the fully showered result and the NLO. We now explain the reason for these differences: with the m_H scale choice the K-factor is near one, and thus the $\bar{B}/B$ amplification that usually enhances the spectrum of the radiated jet (that in this case is the third jet) is not effective. The $\hat{H}_T$ scale is considerably larger than m_H, especially with a large p_T cut, which implies a reduction of the Born cross section and an increase of the K-factor.

In fig. 10 we show the transverse-momentum distribution of the Higgs boson in a Hjj sample with a 20 GeV p_T cut on the two hardest jets. Good agreement is found between the LHE, PY and NLO curves, except for small Higgs transverse momenta, where differences of the order of 30% are found. This is not surprising, in view of the required presence of the two relatively soft jets. Radiation off these jets is Sudakov suppressed in the LHE result with respect to the NLO one. Since this radiation would deplete the jets, the LHE result suffers less depletion, and is thus larger. On the other hand, the shower degrades the energy of the jets lowering the cross section, an effect visible in the PY result. At large Higgs boson p_T, at least one of the jets is forced to be hard, and thus these effects lose importance.

In fig. 11 we show the Higgs boson rapidity distribution in Hjj for p_T cuts of 20, 50 and 100 GeV on the two hardest jets. Again, since this is an inclusive distribution, it displays

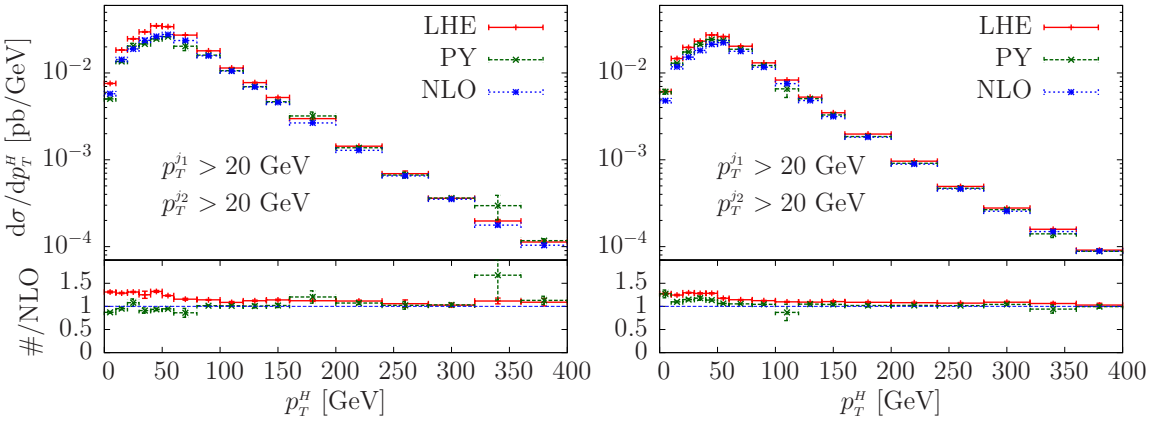

Figure 10: Transverse-momentum distribution of the Higgs boson in a Hjj sample with a 20 GeV p_T cut on the two hardest jets. The left and right plots use respectively the m_H and $\hat{H}_T$ scales.

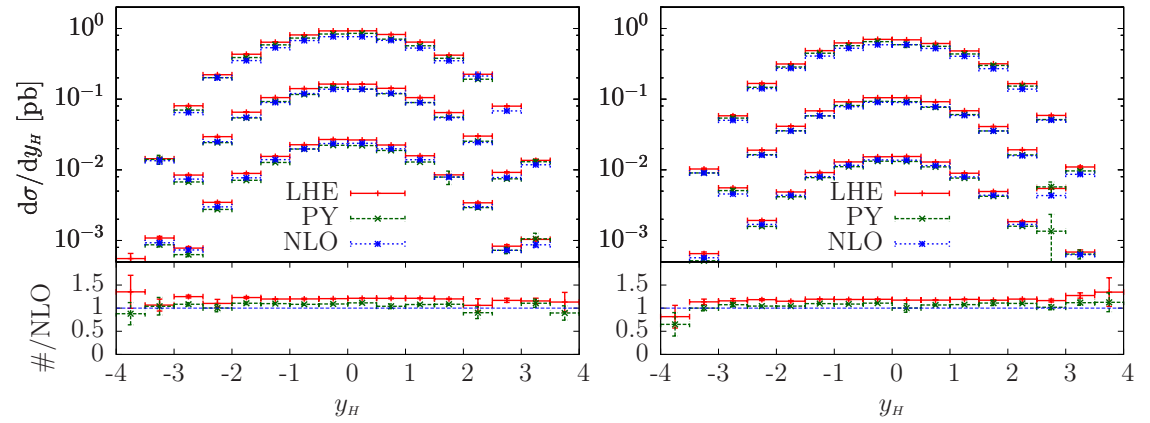

Figure 11: Higgs boson rapidity distribution in Hjj for p_T cuts of 20, 50 and 100 GeV on the hardest jets. The left and right plots use respectively the m_H and $\hat{H}_T$ scales. In the lower pane, the ratio of the LHE and PY results with respect to the NLO one, for the 20 GeV cut.

good agreement between the LHE, PY and NLO results. The ratio is only displayed for the 20 GeV cut. The three predictions become even more consistent for larger p_T cuts, as one would expect.

In figs. 12 and 13 we display the transverse-momentum distribution for the first and second jet. The first distribution bears some similarity to the Higgs transverse momentum, for inclusiveness reasons. Observe that the small momentum disagreement between the LHE and the NLO result observed for the Higgs transverse momentum case is less evident in the hardest jet plot, and even less evident in the second jet one. This is explained by the fact that the same point in the abscissa corresponds to an increasing hardness of the event in the Higgs, first jet and second jet p_T distributions.

Turning to less inclusive quantities, we show in fig. 14 the transverse-momentum distribution of the third hardest jet. We recognize here the typical behaviour of the LHE

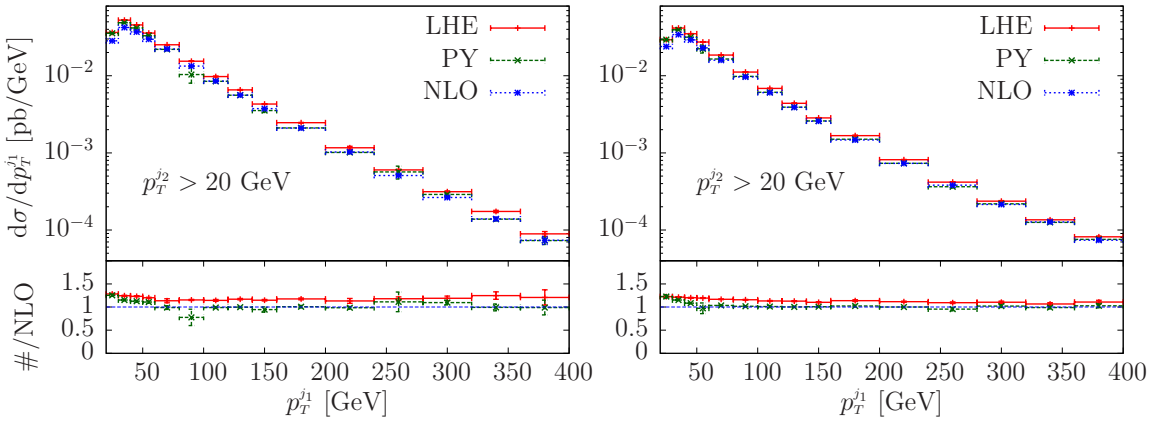

Figure 12: Transverse-momentum distribution of the hardest jet in the Hjj process. The left and right plots use respectively the m_H and $\hat{H}_T$ scales.

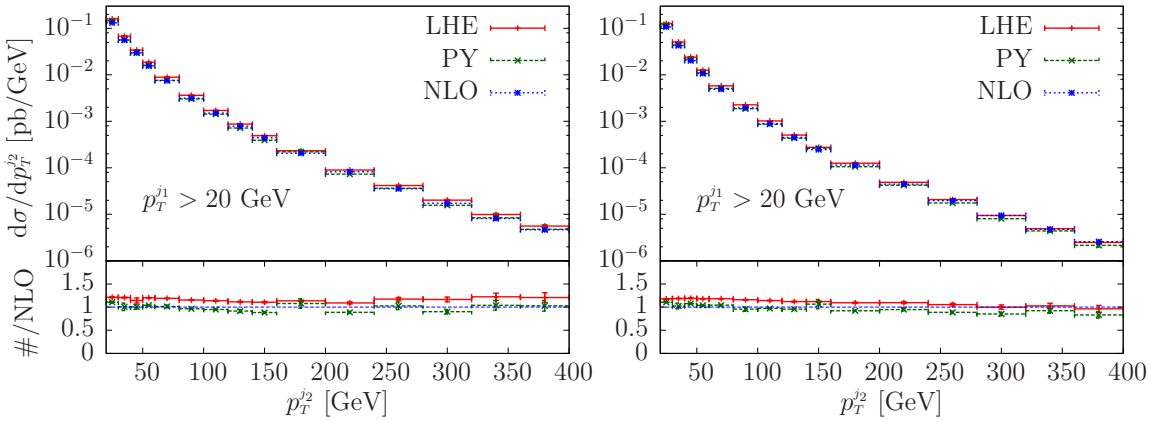

Figure 13: Transverse-momentum distribution of the second hardest jet in the Hjj process. The left and right plots use respectively the m_H and $\hat{H}_T$ scales.

results, with the damping of the small-momentum growth found in the NLO result, and with the typical increase due to the $\bar{B}/B$ factor at higher momenta. As already anticipated in the discussion on the jet multiplicity, we notice that the increase is modest for the m_H choice of scale, but is very large for the $\hat{H}_T$ scale.

In fig. 15 we display the third-jet transverse momentum using three different cuts on the p_T of the first and second jet. The pattern is similar to what was already observed in the Hj case. In the left plot, where the scale is chosen equal to m_H, we see a better concordance of the LHE and NLO results as the transverse momentum increases.

In figs. 16 and 17 we show the $p_T^{\mathrm{rel},j}$ distribution for the hardest and second hardest jet respectively. Here too the pattern is similar to what already observed for the Hj case. The LHE distribution is strongly suppressed, due to the fact that small $p_T^{\mathrm{rel},j}$ values also imply that no initial state radiation has taken place above that scale, and the distribution is dominated by the shower effects, that are not obtained with the same scale choice as the

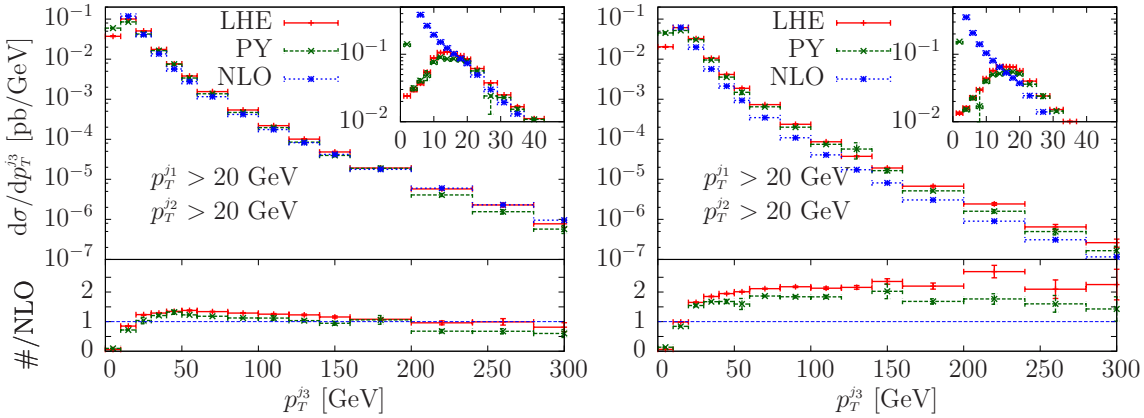

Figure 14: Transverse-momentum distribution of the third hardest jet in the Hjj process. The left and right plots use respectively the m_H and $\hat{H}_T$ scales.

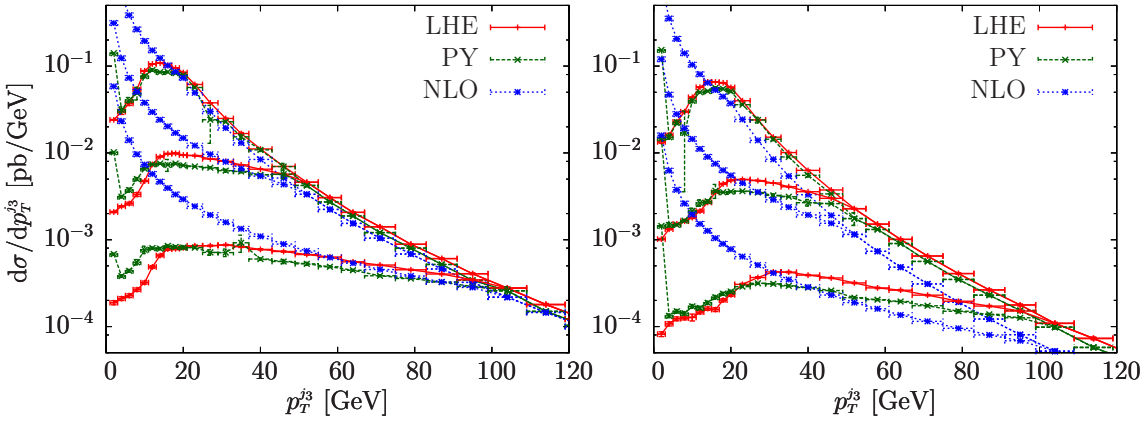

Figure 15: Transverse-momentum distribution of the third hardest jet in the Hjj process for the transverse momentum cut on the two hardest jets equal to 20, 50 and 100 GeV.

NLO result. We can again notice that also the $\bar{B}/B$ K-factor plays a role here, especially for the right plots, that have a larger K-factor because of the use of the $\hat{H}_T$ scale.

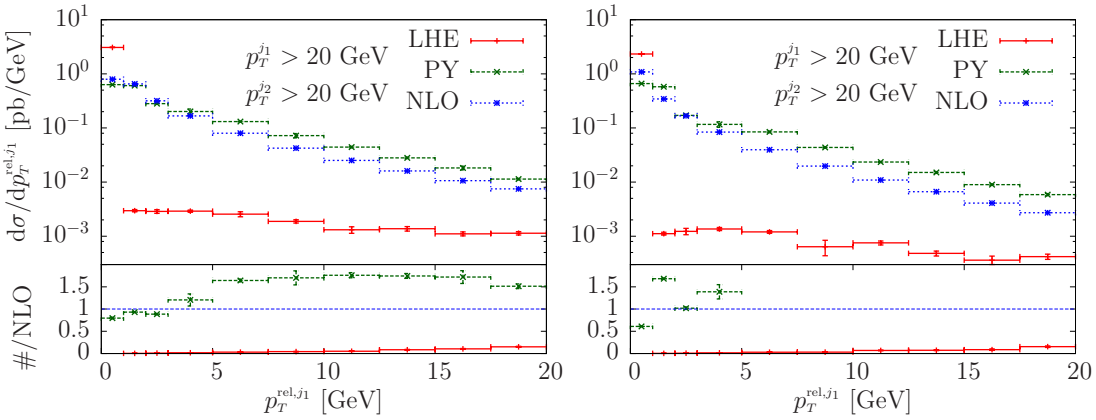

Figure 16: p_T^{rel,j_1} distribution of the hardest jet in the Hjj process. The left and right plots use respectively the m_H and $\hat{H}_T$ scales.

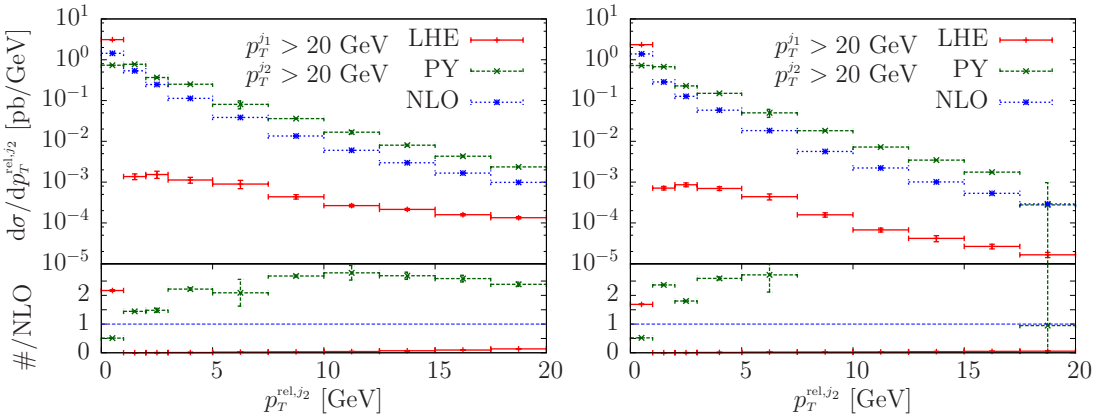

Figure 17: p_T^{rel,j_2} distribution of the second hardest jet in the Hjj process. The left and right plots use respectively the m_H and $\hat{H}_T$ scales.

5.3 Hadronization effects and matching ambiguities

In this section we focus upon two topics: the effects of hadronization and the ambiguities related to matching the LHE result to the shower. In figs. 18 and 19 we display the transverse momentum distribution of the radiated jet for different cuts on the first jet p_T, for the Hj and Hjj generators respectively.

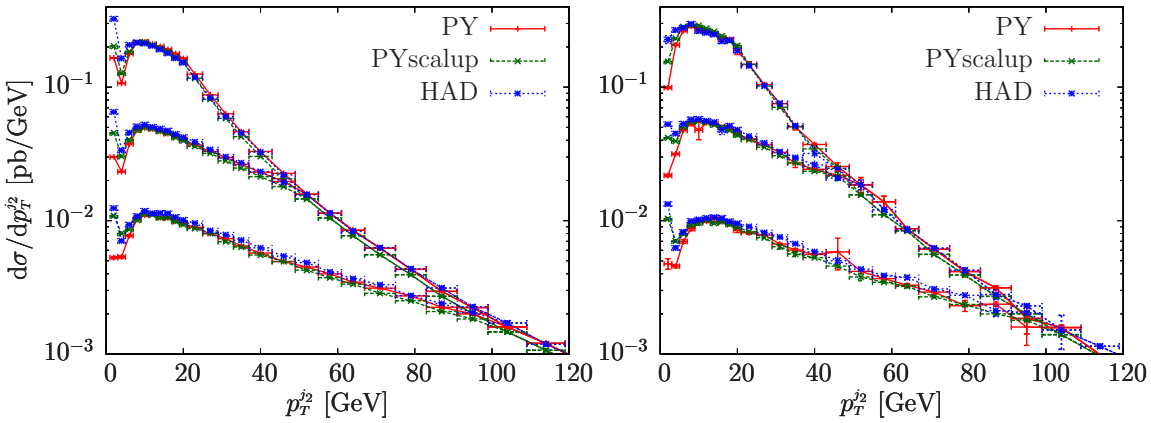

Figure 18: Transverse-momentum distribution of the second hardest jet in the Hj process for the p_T cut on the hardest jet equal to 20, 50 and 100 GeV.

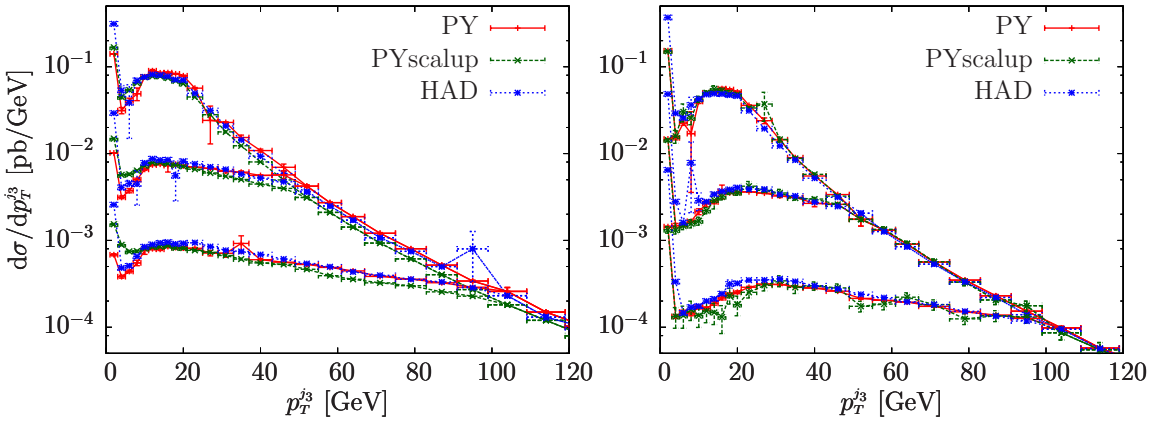

Figure 19: Transverse-momentum distribution of the third hardest jet in the Hjj process for the p_T cut on the two hardest jets equal to 20, 50 and 100 GeV.

The curves labelled "PYscalup" are obtained with a non-default determination of the `scalup` parameter to be set in the Les Houches interface, which limits the hardness of the radiation of the following shower. While normally in `POWHEG` the `scalup` is set to the hardest momentum of the radiation that `POWHEG` generates, in the "PYscalup" results, we determine it by finding the smallest transverse momentum of the LHE, which can be either the transverse momentum of any parton relative to the beam axis, or of any parton relative to any other parton, computed in the center-of-mass frame. Because of the way the real-

radiation contribution is separated into singular contributions, the two choices differ only for subleading configurations, and one expects only a minor effect due to this change. The plots in both figures confirm this expectation. Similarly, we see that hadronization and underlying-event effects (indicated with HAD in the figures) have a sizeable impact on the distributions only for small transverse momenta, as expected.

5.4 Comparison between the H, Hj and Hjj generators

In this section, we compare a few distributions that are described by more than one available POWHEG BOX generator. This comparison can be considered as a first step in the direction of merging POWHEG BOX samples with increasing number of jets.

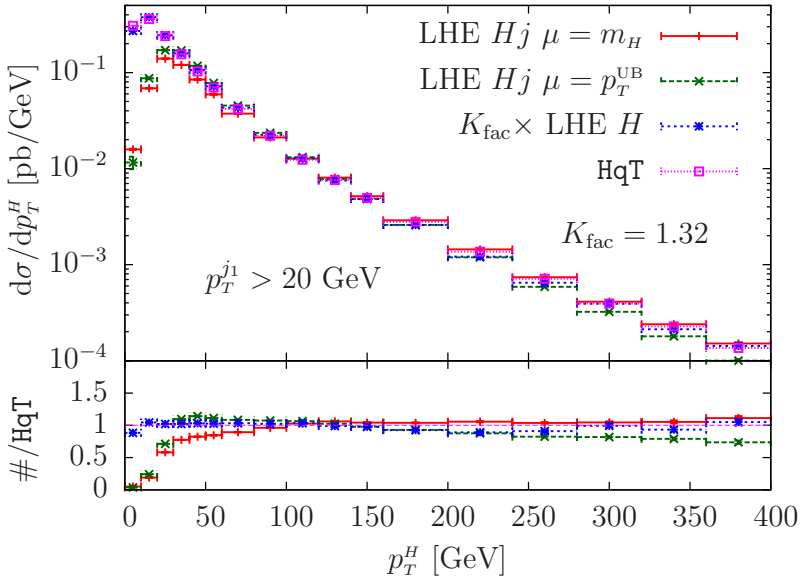

Figure 20: Comparison of the Higgs boson transverse-momentum distribution computed with the H, Hj and HqT generators. The LHE Hj results are shown for the m_H and the Higgs underlying-Borm $p_T^{\rm UB}$ scale choice.

We first consider a comparison between the Higgs boson transverse-momentum spectrum obtained using the H and the Hj generators. The H generator describes this distribution in the whole p_T range, with the Sudakov region obtained with NLL accuracy, and with leading-order accuracy for the high-momentum region. On the other hand, the Hj generator describes this distribution with NLO accuracy, but only for transverse momenta above the Sudakov region.

In these comparisons, the H sample was obtained following the recommendation of ref. [38], i.e. the parameter `hfact` was set to $m_H/1.2$ in the `powheg.input` file. With this setup, the resulting Higgs boson p_T distribution is in remarkable agreement with the output of the HqT program [39, 40, 41, 42]. Furthermore, we apply a K-factor of 1.32 to the H result, in order to match the HqT total NNLO cross section ($\sigma_H^{\rm NLO} = 10.85$ pb, $\sigma_H^{\rm NNLO} = 14.35$ pb). The results are displayed in fig. 20. The two figures differ only for the scale choice used in the Hj generator, since HqT accepts only a fixed renormalization and

factorization scale. As one can see, the agreement of the rescaled H and HqT generators is excellent, as remarked in ref. [38]. The Hj generator, using as scale the Higgs boson mass, is also in excellent agreement with HqT for large transverse momenta. This is not surprising, since, in this kinematic region, it is using the same $\mathcal{O}(\alpha_S^4)$ result of HqT, and furthermore it is using the same factorization and renormalization scale. At low p_T, the Hj results begin to feel the lack of soft-gluon resummation effects that are included in HqT. The Hj result computed with the dynamical scale shows a substantially similar pattern, undershooting the HqT one by $20 \div 25\%$, a difference that is easily explained as being due to the different scale adopted in the Hj program and in HqT.

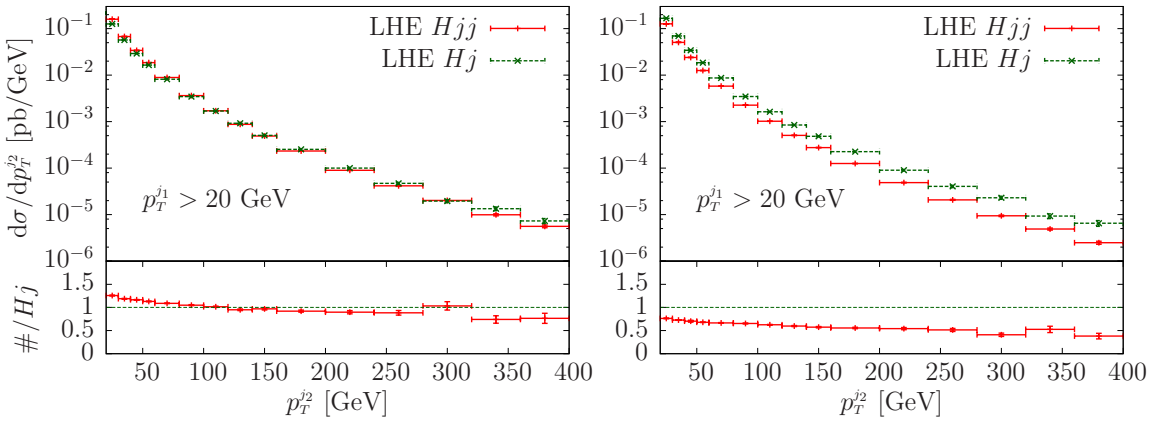

Figure 21: Comparison of the second hardest jet transverse momentum computed with the Hj and Hjj generators. The left plot uses the m_H scale in both the Hj and Hjj generators. In the right plot the Hj generator uses the Higgs underlying-Born transverse momentum scale, while the Hjj generator uses $\hat{H}_T$.

Turning to the comparison of the Hj and Hjj generators for the transverse-momentum distribution of the second hardest jet, we notice that the Hj generator computes this distribution down to small values of the transverse momentum, since it includes the appropriate Sudakov effects. At large transverse momenta, however, it only has leading-order accuracy. The Hjj program has instead NLO accuracy at large transverse momenta, but does not include fully resummed Sudakov effects at small p_T. We do not have any higher-accuracy calculation for this distribution, as in the previous case. The results are displayed in fig. 21. Notice that, for the m_H scale choice, the matching is very good, something that we expect since the K-factor is close to one in this case. Matching with the running scales leads, instead, to non-negligible differences, although a stability plateau is present roughly above 60 GeV, and for not too large values of the transverse momentum.

6. Conclusions

In the present work we have developed generators for the gluon fusion production of a Higgs boson in association with one or two jets. We have examined the output of the two generators, comparing them with fixed order NLO calculations, among each other, and

with the fully inclusive $gg \to H$ POWHEG generator. The features of the distributions we have examined are all well understood, and reflect our expectations for a typical POWHEG generator. In general, we find that quantities inclusive in the radiated jet (i.e. the second jet in $gg \to H + 1\,\text{jet}$ and the third jet in $gg \to H + 2\,\text{jets}$) are in good agreement with the fixed order NLO result, while ditributions in the radiated jet reflect the features of Sudakov suppression and NLO enhancement that are typical of NLO results matched with shower generators. We see no indication of problems related to the increase in complexity when going from the inclusive Higgs production to the associated production with one and two jets, other than an increased requirement of computer time.

The development of the Higgs production code has been achieved using a new interface to the MadGraph4 code, that has also been presented in this work. The use of this interface has considerably simplified the construction of the generator. The interface is fully generic, and so we expect that the implementation of new processes will be greatly simplified with its use.

The code of our new Higgs production generators can be accessed via the POWHEG BOX svn repository see the POWHEG web page http://powhegbox.mib.infn.it for instructions). The new MadGraph4 interface is also available there, so that people willing to develop their own POWHEG code may benefit from its use.

A. The interface with MadGraph4: technical details

The MadGraph4 interface is available under the POWHEG-BOX/MadGraphStuff directory. To use the interface, create a process directory in the POWHEG-BOX directory, and copy the whole content of the MadGraphStuff directory to this new process directory. To specify the process, edit the file Cards/proc_card.dat and set the process and the physics model as in MadGraph4. Always enter the real emission process, i.e. the Born process plus an extra jet j. For example, to generate Higgs boson plus two jets at a proton-proton collider, we entered

```
p p > H j j j
QCD=3
QED=0
HIG=1
```

It is recommended to set the parameters QCD and QED to be exactly equal to the number of strong and electroweak interactions in the real-emission process (excluding the couplings present in the effective vertex, if any). In the case of the heft model (see below), it is also needed to set the parameter HIG=1 to allow for the effective Higgs boson to gluon coupling to be included in the Feynman diagrams.

The ordering of the particles in the process should follow the POWHEG BOX conventions:

1. first particle: incoming particle with positive rapidity

2. second particle: incoming particle with negative rapidity

3. from the third particle onward: final-state particles ordered as follows

    - colourless particles first,
    - massive coloured particles,
    - massless coloured particles.

The default MadGraph4 interface has been validated to work with the following three physics models:

- sm: This is the default MadGraph4 model with a massive top and bottom quarks, diagonal CKM matrix and massless electrons and muons.
- smckm: This is the same as the sm model, however, the full CKM matrix can be specified in the parameter card.
- heft: This is the same as the default sm model with the inclusion of the effective coupling between gluons and the Higgs boson in the large top-quark mass limit. The Higgs Yukawa interaction with bottom quarks is neglected in this model.

Although the interface has not been tested with other physics models, it is straight-forward to extend the interface to work with any simple extension of the Standard Model.

To generate the process, execute the NewProcess.sh script. This will compile the MadGraph4 code, generate the (correlated) Born and real-emission squared amplitudes and create the libraries that can be linked to the POWHEG BOX. In particular, libmadgraph.a contains the matrix elements, libdhelas3.a the HELAS library and libmodel.a the physics model. Furthermore, the following files are written in the current directory:

- Born.f: it contains the routines setborn to compute the (correlated) Born squared matrix elements and borncolour_lh that assigns the colour flow to a Born process.
- real.f: it contains the routines setreal to compute the real-emission squared matrix elements.
- Cards/param_card.dat: this is the input card where all the model parameters need to be specified.
- init_couplings.f: this contains the init_couplings routine that sets all the model parameters specified in the param_card.dat. The coupling constants that depend on the strong coupling st_alpha or from the event kinematics should be specified in the routine set_ebe_couplings, that is updated event-by-event.
- coupl.inc: it contains the common blocks for all the couplings used by MadGraph4.

To complete the implementation of a process in the POWHEG BOX, the user must provide the Born phase-space in the file Born_phsp.f and the virtual squared matrix elements in the file virtual.f. Also, no information on possible intermediate resonances in the matrix elements is kept. The user needs to specify explicitly in the routine finalize_lh (in the

Born.f file) which resonances should be written in the LHE file, so that the shower Monte Carlo program can deal with them correctly. Finally, the resulting code can be compiled by executing the command

```
$ make pwhg_main
```

B. PYTHIA setup

References

[1] A. Collaboration, *Combined search for the Standard Model Higgs boson using up to 4.9 fb^{-1} of pp collision data at $\sqrt{s} = 7$ TeV with the ATLAS detector at the LHC*, arXiv:1202.1408.

[2] **CMS Collaboration** Collaboration, S. Chatrchyan *et. al.*, *Combined results of searches for the standard model Higgs boson in pp collisions at $\sqrt{s} = 7$ TeV*, arXiv:1202.1488.

[3] D. Zeppenfeld, R. Kinnunen, A. Nikitenko, and E. Richter-Was, *Measuring Higgs boson couplings at the LHC*, *Phys. Rev.* **D62** (2000) 013009, [hep-ph/0002036].

[4] M. Duhrssen, S. Heinemeyer, H. Logan, D. Rainwater, G. Weiglein, *et. al.*, *Extracting Higgs boson couplings from CERN LHC data*, *Phys.Rev.* **D70** (2004) 113009, [hep-ph/0406323].

[5] T. Plehn, D. L. Rainwater, and D. Zeppenfeld, *Determining the structure of Higgs couplings at the LHC*, *Phys. Rev. Lett.* **88** (2002) 051801, [hep-ph/0105325].

[6] J. M. Campbell, R. Ellis, and C. Williams, *Hadronic production of a Higgs boson and two jets at next-to-leading order*, *Phys.Rev.* **D81** (2010) 074023, [arXiv:1001.4495].

[7] J. M. Campbell, R. K. Ellis, and G. Zanderighi, *Next-to-leading order higgs + 2 jet production via gluon fusion*, *JHEP* **10** (2006) 028, [hep-ph/0608194].

[8] S. Hoeche, F. Krauss, M. Schonherr, and F. Siegert, *A critical appraisal of NLO+PS matching methods*, arXiv:1111.1220.

[9] S. Alioli, P. Nason, C. Oleari, and E. Re, *A general framework for implementing NLO calculations in shower Monte Carlo programs: the POWHEG BOX*, *JHEP* **06** (2010) 043, [arXiv:1002.2581].

[10] http://mcfm.fnal.gov.

[11] T. Stelzer and W. F. Long, *Automatic generation of tree level helicity amplitudes*, *Comput. Phys. Commun.* **81** (1994) 357–371, [hep-ph/9401258].

[12] J. Alwall *et. al.*, *MadGraph/MadEvent v4: The New Web Generation*, *JHEP* **09** (2007) 028, [arXiv:0706.2334].

[13] H. Murayama, I. Watanabe, and K. Hagiwara, *Helas: Helicity amplitude subroutines for feynman diagram evaluations*, . KEK-91-11.

[14] R. Frederix, T. Gehrmann, and N. Greiner, *Automation of the Dipole Subtraction Method in MadGraph/MadEvent*, *JHEP* **09** (2008) 122, [arXiv:0808.2128].

[15] R. Frederix, T. Gehrmann, and N. Greiner, *Integrated dipoles with MadDipole in the MadGraph framework*, *JHEP* **1006** (2010) 086, [arXiv:1004.2905].

[16] T. Gehrmann and N. Greiner, *Photon Radiation with MadDipole*, *JHEP* **1012** (2010) 050, [arXiv:1011.0321].

[17] R. Frederix, S. Frixione, F. Maltoni, and T. Stelzer, *Automation of next-to-leading order computations in QCD: the FKS subtraction*, *JHEP* **10** (2009) 003, [arXiv:0908.4272].

[18] F. Wilczek, *Decays of Heavy Vector Mesons Into Higgs Particles*, *Phys.Rev.Lett.* **39** (1977) 1304.

[19] A. Djouadi, M. Spira, and P. Zerwas, *Production of Higgs bosons in proton colliders: QCD corrections*, *Phys.Lett.* **B264** (1991) 440–446.

[20] S. Dawson, *Radiative corrections to Higgs boson production*, *Nucl.Phys.* **B359** (1991) 283–300.

[21] C. F. Berger, V. Del Duca, and L. J. Dixon, *Recursive Construction of Higgs-Plus-Multiparton Loop Amplitudes: The Last of the Phi-nite Loop Amplitudes*, *Phys.Rev.* **D74** (2006) 094021, [hep-ph/0608180].

[22] S. Badger and E. Glover, *One-loop helicity amplitudes for $H \to$ gluons: The All-minus configuration*, *Nucl.Phys.Proc.Suppl.* **160** (2006) 71–75, [hep-ph/0607139].

[23] S. Badger, E. Glover, and K. Risager, *One-loop phi-MHV amplitudes using the unitarity bootstrap*, *JHEP* **0707** (2007) 066, [arXiv:0704.3914].

[24] E. Glover, P. Mastrolia, and C. Williams, *One-loop phi-MHV amplitudes using the unitarity bootstrap: The General helicity case*, *JHEP* **0808** (2008) 017, [arXiv:0804.4149].

[25] S. Badger, E. Nigel Glover, P. Mastrolia, and C. Williams, *One-loop Higgs plus four gluon amplitudes: Full analytic results*, *JHEP* **1001** (2010) 036, [arXiv:0909.4475].

[26] L. J. Dixon and Y. Sofianatos, *Analytic one-loop amplitudes for a Higgs boson plus four partons*, *JHEP* **0908** (2009) 058, [arXiv:0906.0008].

[27] S. Badger, J. M. Campbell, R. K. Ellis, and C. Williams, *Analytic results for the one-loop NMHV Hqqgg amplitude*, *JHEP* **0912** (2009) 035, [arXiv:0910.4481].

[28] S. Frixione, P. Nason, and C. Oleari, *Matching NLO QCD computations with Parton Shower simulations: the POWHEG method*, *JHEP* **11** (2007) 070, [arXiv:0709.2092].

[29] P. Nason, *MINT: A Computer program for adaptive Monte Carlo integration and generation of unweighted distributions*, arXiv:0709.2085.

[30] S. Alioli, K. Hamilton, P. Nason, C. Oleari, and E. Re, *Jet pair production in POWHEG*, *JHEP* **04** (2011) 081, [arXiv:1012.3380].

[31] J. Pumplin *et. al.*, *New generation of parton distributions with uncertainties from global QCD analysis*, *JHEP* **07** (2002) 012, [hep-ph/0201195].

[32] A. D. Martin, W. J. Stirling, R. S. Thorne, and G. Watt, *Parton distributions for the LHC*, *Eur. Phys. J.* **C63** (2009) 189–285, [arXiv:0901.0002].

[33] **NNPDF** Collaboration, R. D. Ball *et. al.*, *A determination of parton distributions with faithful uncertainty estimation*, *Nucl. Phys.* **B809** (2009) 1–63, [arXiv:0808.1231].

[34] M. Cacciari, G. P. Salam, and G. Soyez, *The anti-k_T jet clustering algorithm*, *JHEP* **04** (2008) 063, [arXiv:0802.1189].

[35] S. Alioli, P. Nason, C. Oleari, and E. Re, *NLO Higgs boson production via gluon fusion matched with shower in POWHEG*, *JHEP* **04** (2009) 002, [arXiv:0812.0578].

[36] P. Nason, *Recent developments in POWHEG*, *PoS* **RADCOR2009** (2010) 018, [arXiv:1001.2747].

[37] P. Nason and B. Webber, *Next-to-Leading-Order Event Generators*, arXiv:1202.1251.

[38] S. Dittmaier, S. Dittmaier, C. Mariotti, G. Passarino, R. Tanaka, *et. al.*, *Handbook of LHC Higgs Cross Sections: 2. Differential Distributions*, arXiv:1201.3084. Report of the LHC Higgs Cross Section Working Group.

[39] *http://theory.fi.infn.it/grazzini/codes.html*.

[40] G. Bozzi, S. Catani, D. de Florian, and M. Grazzini, *The q_T spectrum of the Higgs boson at the LHC in QCD perturbation theory*, *Phys.Lett.* **B564** (2003) 65–72, [hep-ph/0302104].

[41] G. Bozzi, S. Catani, D. de Florian, and M. Grazzini, *Transverse-momentum resummation and the spectrum of the Higgs boson at the LHC*, *Nucl.Phys.* **B737** (2006) 73–120, [hep-ph/0508068].

[42] D. de Florian, G. Ferrera, M. Grazzini, and D. Tommasini, *Transverse-momentum resummation: Higgs boson production at the Tevatron and the LHC*, *JHEP* **1111** (2011) 064, [arXiv:1109.2109].